Bimetallic Metal-Organic Framework Fe/Co-MIL-88(NH₂)

Exhibiting High Peroxidase-like Activity and Its Application in

Detection of Extracellular Vesicles

Qiaoshi Jiang,¹ Yuchen Xiao,² Anh N. Hong,² Ziting Gao,² Yuyang Shen,¹ Qingsong Fan,² Pingyun Feng^{2,*} and Wenwan Zhong^{1,2,*}

¹Environmental Toxicology Graduate Program; ²Department of Chemistry, University of California-Riverside, Riverside, CA 92521, U.S.A.

ABSTRACT

Metal–organic frameworks (MOFs) have many attractive features, including tunable composition, rigid structure, controllable pore size, and large specific surface area, and thus are highly applicable in molecular analysis. Depending on the MOF structure, a high number of un-saturated metal sites can be exposed to catalyze chemical reactions. In the present work, we report that by using both Co(II) and Fe(III) to prepare the MIL-88(NH₂) MOF, we can produce the bimetallic MOF that can catalyze the conversion of 3,3', 5,5"-tetramethylbenzidine (TMB) to a color product through reaction with H₂O₂ at a higher reaction rate than the monometallic Fe-MIL-88(NH₂). The Michaelis constants (K_m) of the catalytic reaction for TMB and H₂O₂ are 3-5 times smaller, and the catalytic constants (k_{cat}) are 5-10 times higher than those of the horse-radish peroxidase (HRP), supporting ultrahigh peroxidase-like activity. These values are also much more superior to those of the HRP-mimicking MOFs reported previously. Interestingly, the bimetallic MOF can be coupled with glucose oxidase (GOx) to trigger the cascade enzymatic reaction for highly sensitive detection of extracellular vesicles (EVs), a family of important biomarkers. Through conjugation

to the aptamer that recognizes the marker protein on EV surface, the MOF can help isolate the EVs from biological matrices, which are subsequently labeled by GOx via antibody recognition. The cascade enzymatic reaction between MOF and GOx enables detection of EVs at a concentration as low as 7.8×10^4 particles/ml. The assay can be applied to monitor EV secretion by cultured cells, and also can successfully detect the different EV quantities in the sera samples collected from cancer patients and healthy controls. Overall, we prove that the bimetallic Fe/Co-MIL-88(NH₂) MOF, with its high peroxidase-activity and high biocompatibility, is a valuable tool deployable in clinical assays to facility disease diagnosis and prognosis.

KEYWORDS: Metal-organic frameworks; Peroxidase-like activity; Extracellular vesicles; Cascade enzymatic reaction; Glucose oxidase; Colorimetric detection; Steady-state kinetic analysis

INTRODUCTION

Metal–organic frameworks (MOFs) are porous crystalline materials constructed from metal ions or metal cluster nodes and organic linkers with high regularity of coordination bonds. They can be formed from diverse metal cations like Cu²⁺, Co²⁺, Fe³⁺, Ga³⁺, etc., and ligands like carboxylates, phosphonates, or N-donating azolate linkers. By changing the type and ratio of the metal and ligand in the MOF frameworks, their structures and pore sizes can be tuned. Their tunable physicochemical properties and porous structures permit MOFs to be employed in many areas, such as catalysis, gas storage and separation, energy production and conversion. 4,5

In recent years, their application scope has been expanded to biomedical sensing and imaging, taking advantage of their reversible metal-ligand coordination structure and high loading capacity.^{6, 7} Most interestingly, the tailorable cavities with a high number of exposed unsaturated metal sites and channels formed from diverse metal nodes and bridging linker in MOFs mimic the coordination environment and electron transfer routes in natural enzymes.^{8, 9} Several types of MOFs have been discovered to possess intrinsic peroxidase-mimicking catalytic activity, including the zeolitic imidazolate frameworks (ZIFs), the Fe-based MIL-MOFs (MIL = Material Institute of Lavoisier), the Zr-based UiO-MOFs (UiO = University of Olso), the Cu-based HKUST-MOFs (HKUST = Hong Kong University of Science and Technology), the Ni-based MOFs, MIL101 (Fe, Co)@MIP, and the Prussian blue-based MOFs. 10-14 These MOF-based peroxidase mimics often contain transition metals like Fe, Co, Ni, Cu, etc., because such metals can catalyze generation of free radicals. For example, Fe can catalyze the Fenton reaction that produces hydroxyl radicals from H₂O₂. Superior to the biological enzymes, like horseradish peroxidase (HRP) employed in enzyme-linked immunosorbent assay (ELISA), MOFs have highly tunable catalytic activity and can be synthesized at lower costs in a larger scale, 15-17 attracting great attention in biosensing.

Extracellular vesicles (EVs) secreted by almost all types of cells carry diverse cargo molecules like proteins, nucleic acids, and lipids, and play pivotal roles in cell-cell communication. ¹⁸⁻²² They present in biological fluids, ^{23, 24} and can impact pathological developments associated with immune responses, viral pathogenicity, cancer progression, and cardiovascular or central nervous system–related diseases. ²⁵⁻²⁸ Both their close association with disease development and easy accessibility in the circulation systems support the high potential of EVs as diagnostic and therapeutic markers. However, the concentration of EVs with good potential to be disease markers in biological samples could be very low, ²⁹ making it very challenging to detect such EVs using conventional methods like ELISA, Western Blotting (WB), and flow cytometry (FCM). ³⁰ State-of-the-art sensors built on microfluidic and nanofluidic devices have been developed to detect EVs down to 100 particles/mL. ^{29, 31-36} Still, simple but sensitive techniques for rapid EV detection are in demand to speed up the discovery and clinical applications of the EV-based disease markers.

Herein, a bimetallic MIL-88 MOF was synthesized by using 2-aminoterephthalate as the ligand and both Fe and Co as metal cations. This bimetallic Fe/Co-MIL-88(NH₂) shows high peroxidase-like activity and high dispersity in aqueous solutions. It can act as the peroxidase-mimic and work together with glucose oxidase (GOx) in the cascade enzymatic reactions to oxidize the peroxidase substrate by inputting glucose. This reaction system can be used for sensitive EV detection in biological samples, and acquire the detection limit two orders of magnitude lower than that obtained with HRP, proving the feasibility of the peroxidase-mimicking bimetallic MOFs being promising tools in liquid biopsy.

EXPERIMENTAL SECTION

Materials. Ferric chloride, 6-hydrate (FeCl₃ · 6H₂O, 98.1%) was acquired from J. T. Baker (Phillipsburg, NJ). Sodium chloride, potassium phosphate dibasic salt (anhydrous), acetic acid, N, N-dimethylformamide (DMF) and cobalt(II) nitrate hexahydrate (Co(NO₃)₂ · 6H₂O, 99%) were purchased from Fisher Scientific (Waltham, MA). 2-Aminoterephthalic acid (H₂(NH₂)BDC), TMB (3,3', 5,5"-tetramethylbenzidine), polyethylene glycol 400, potassium chloride, glycine (for electrophoresis, ≥99%) and glutaraldehyde solution were from Sigma-Aldrich (Saint Louis, MI). Ethanol (EtOH, Anhydrous) was from KOPTEC. The amino group modified CD63 aptamer was produced by IDT, Inc. (Coralville, IA). The mouse anti-human CD9 (Clone MM2/57) and HRP were obtained from Sino Biological (Beijing, China) and Cell Signaling Technology (Danvers, MA), respectively. Streptavidin was purchased from Thermo Fisher Scientific (Waltham, MA). All chemicals were at the analytical reagent grade and used without further purification. Ultrapure water with electric resistance > 18.2 MΩ was produced by the Milipore Milli-Q water purification system (Billerica, MA).

Synthesis and activation of Fe-MIL-88(NH₂) and Fe/Co-MIL-88(NH₂). The MOF materials were prepared via a solvothermal method. In a typical approach for production of the bimetallic Fe/Co-MIL-88(NH₂), 0.082 g FeCl₃ · 6H₂O, 0.090 g Co(NO₃)₂ · 6H₂O, and 0.053 g H₂(NH₂)BDC were dissolved in 3.181 g DMF in a 23 mL glass bottle, stirred for 40 min, and then heated in 120 °C for 24 hours. After cooling down to room teperature, the brown-color crystal Fe/Co-MIL-88(NH₂) were washed with DMF, collected by centrifugation, and dried at room temperature. The monometalic Fe-MIL-88(NH₂) was synthesized in the same way, but by mixing 0.163 g FeCl₃ · 6H₂O and 0.057 g H₂(NH₂)BDC in 3.058 g DMF, and heated in 140 °C. Both MOF crystals were washed twice with ethanol at 60 °C or room temperature, and then dried by

vacuum to remove the residual DMF that may impede with the subsequent enzyme activity measurement and sensing performance.

Powder X-ray Diffraction (PXRD) Characterization. The phase purity of Fe-MIL-88(NH₂) and Fe/Co-MIL-88(NH₂) was examined by powder X-ray diffraction on a PANalytical Empyrean Series 2 diffractometer operated at 45 kV and 40 mA (Cu Kα radiation, λ = 1.5418 Å). The data collection was performed at room temperature in the range from 5° to 40° with a step size of ~0.026°. The simulated Fe-MIL-88(NH₂) powder pattern was obtained from the Fe-MIL-88(NH₂) single crystal data.³⁷

Peroxidase-like activity evaluation of Fe/Co-MIL-88(NH₂) and Fe/Co-MIL-88(NH₂). The peroxidase-like activity of the two MOF materials was evaluated using the reaction between H₂O₂ and 3,3′,5,5′-tetramethylbenzidine (TMB). In brief, 50 μg/mL MOF, 1 mM TMB, and H₂O₂ at various concentrations (0, 0.005, 0.05, 0.1, 0.5 and 1 mM) were added to 0.4 mL of 200 mM NaAc-HAc buffer (pH 4.1). The mixture was incubated at 37° C for 15 min, and the visible light absorbance at 652 nm of the TMB oxidation product, i.e. oxTMB, was read in the synergy HT microplate reader.

Enzyme Kinetics Analysis of activated Fe/Co-MIL-88(NH₂). The steady-state kinetics assays were performed as follows. The activated Fe/Co-MIL-88(NH₂) at the concentration of 50 μg/ml in 100 μL of 200 mM NaAc-HAc buffer (pH 4.1) was incubated with 1.0 mM TMB and H₂O₂ at various concentrations (0, 0.05, 0.1, 0.5, 1.0, and 10 mM) at 37°C. A time-course mode was used to monitor the absorbance change at 652 nm with a 10 s interval for 15 min in the synergy HT microplate reader. The Beer–Lambert law was used to convert the absorbance to oxTMB concentration using the molar absorptivity at 652 nm of oxTMB (39,000 M⁻¹ · cm⁻¹)³⁸ and the

optical length of 0.233 cm of the 96-well plates. The slope of the concentration change within the first 15 min was then calculated to represent the initial velocity (V).

Preparation of Fe/Co-MIL-88(NH₂)/Aptamer Bioconjugate. Aptamer conjugation started by dispersing 35 mg Fe/Co-MIL-88(NH₂) in 20 ml 1× PBS, followed by addition of 100 μl glutaraldehyde. After stirring the solution for 2 hours, the solid was centrifuged down, washed with 1× PBS for 2 times, and dispersed in 2 ml 1× PBS. Next, 10 μL of 0.10 mM aptamer was added to the mixture and the solution was put on a rotating plate and shaken overnight. The Fe/Co-MIL-88(NH₂)/ aptamer conjugate was then collected by centrifugation (20,000 g, 3 min), and redispersed in 2 ml of 0.1 M glycine buffer containing 8 mM PEG for 1 hour to passivate the MOF surface.

Cell culture and EV collection. HeLa cells (HeLa ATCC® CCL- 2^{TM}) were cultured in DMEM medium (Corning) containing 10% fetal bovine serum (FBS, Gibco) and 1% penicillin/streptomycin (Corning). All cell lines were maintained at 37 °C in a humidified 5% CO₂ incubator and routinely screened for Mycoplasma contamination. EV harvest was carried out by a SorvallTM ST 16 Centrifuge (Thermo Fisher Scientific) and an Optima XPN-80 ultracentrifuge (Beckman Coulter). The medium was replaced with the EV-depleted culture medium after the cells reached a confluency of 75%. The cells were cultured for 24-48 hours in this medium, which was then centrifuged at 500 g for 15 min to sediment the cells, and another 20-min centrifugation at 15,000 g to remove the remaining cellular debris. Next, the medium was ultra-centrifuged at 110,000 g for 70 min to harvest the EVs released by the cells. The EV pellet was washed once and re-suspended in the freshly prepared 1× PBS. The EV solution was used within three days of preparation.

Detection of EV relying on the HRP-mimicking activity of Fe/Co-MIL-88(NH₂). Twenty μl of the EV sample was mixed with 170 μl of the Fe/Co-MIL-88(NH₂)/aptamer bioconjugate at 17.5 mg/mL and 10 μl of the biotin-anti-CD9 antibody solution at 0.10 mg/ml. The mixture was shaken at room temperature for 3 hrs. The Fe/Co-MIL-88(NH₂)/aptamer -EV-anti-CD9 antibody was centrifuged down (20,000 g, 3 min) and resuspended in 100 μl of the streptavidin solution at 17 μg/ml. After 1-hour incubation, the product was centrifuged down (20,000g, 3 min), washed with 1×PBS for 1 time, and mixed with 100 μl biotin-GOx at 0.013 mg/ml. After two washes with 1×PBS, the final product was resuspended in 30 μl 1× PBS, 20 μl of which was mixed with 5 μl TMB (40 mM), 5 μl glucose (40 mM) and 370 μl NaAc-HAc buffer and incubated in 37 °C for 1 hour. With the MOF bioconjugates removed by centrifugation, the clear solution was tested in the synergy HT microplate reader (BioTek Instruments, Inc.).

RESUTLS AND DISCUSSION

Design and characterization of bimetallic Fe/Co-MIL-88(NH₂) MOFs. For reliable applications of the MOF-based peroxidase mimics, dispersity and stability in aqueous solution are critical.³⁹ The Fe-based MIL-88 MOF has high aqueous compatibility because it uses hydrophilic bridging ligands like 2-aminoterephthalic acid, which also bring in the benefit of easy conjugation with biomolecules like antibodies.^{40,41} It has also been reported to possess peroxidase-like activity. The porous structure of MIL-88 exposes plenty of Fe(III) on surface that can serve as the activity centers to catalyze the heterogeneous Fenton reactions at the solid/liquid interface. In aqueous solutions, the unsaturated, open iron sites can be terminated by water or hydroxide.^{42,43} If these non-bridging ligands are replaced by the Lewis base H₂O₂, Fe(III) can be reduced to Fe(II),^{44,45} which then reacts directly with H₂O₂ to generate hydroxyl radicals. In addition, incorporating the

Fe-based reaction sites in the solid MOF structures can help prevent rapid diffusion of the iron ions and the radicals in the bulk solution during the Fe(III)/Fe(II) conversion cycles, 9,44 enhancing the catalytic activity.

However, the rate of conversion of Fe(III) to Fe(II) is much slower than that of hydroxyl radical generation by Fe(II) reacting with H₂O₂, limiting its catalytic power.⁴⁶ Other transition metals can trigger Fenton-like reactions as well. For example, Co(II) can be oxidized by H₂O₂ to produce hydroxyl radicals and Co(III)OH, which can be recycled back to Co(II) to generate more radicals.^{47, 48} The standard redox potential of the Co(III)/Co(II) pairs is 1.3 V, higher than that (0.771 V) of the Fe(III)/Fe(II) pairs.^{48, 49} Some Co-based nanozymes have been reported and exhibited high catalytic activity.^{50, 51} Preparation of mixed metal MOFs having Fe in combination with other transition metals like Co and Zn have been proved to be possible.⁵² We thus hypothesize that, adding Co(II) to the Fe-based MIL-88 MOF could improve its peroxidase-mimicking activity, while maintaining its biocompatibility (**Figure 1a**).

The bimetallic Fe/Co-MIL-88(NH₂) was synthesized by the solvothermal method,⁴⁰ as described in the Experimental Section. Fe(III) and Co(II) can coordinate with the carboxyl groups on the NH₂BDC²⁻ ligands, forming the trinuclear transition metal (TM) clusters (TM = Fe and Co) (**Figure 1a**). The Fe-MIL-88(NH₂) was also prepared with the same procedure for activity comparison. Because adding a second metal ion may affect the final morphology of MIL-88 and reduce its stability, we varied the mole ratio of Fe : Co used during the synthesis to see at what ratio a stable bimetallic structure can be obtained. We found that with the input ratio at 1:1, the synthesized Fe/Co-MIL-88(NH₂) MOF exhibited a hexagonal rod-like morphology with a lateral length of about 700 – 1,100 nm and an average diameter of 500 nm when examined by TEM (**Fig. 1b**). DLS measurement showed that the average hydrodynamic diameter of the Fe/Co-MIL-

88(NH₂) was around 600 nm, similar to Fe-MIL-88(NH₂) (Fig. 1c). PXRD was also performed to characterize the crystal structure. The peaks of the Fe/Co-MIL-88(NH₂) matched well with those of the simulated Fe-MIL-88(NH₂) spectrum which confirmed the MIL-88 topology (Fig. 1d). Small variations between the actual and simulated XRD spectra were observed: the flexibility of the MIL-88 architecture could lead to changes in peak position and shape. 53-55 Furthermore, we carried out EDS line scanning (Figure S1), and confirmed the coexistence of Fe (0.70 keV) and Co (0.77 keV) in the Fe/Co-MIL-88(NH₂) framework. The atomic% of Fe and Co was found to be 7.18 % and 2.23 %, respectively, although the mole ratio of the two metals was 1:1 when added to the synthesis solution. Fe(III) is a harder Lewis acid compared to Co(II), and can bind more easily to the carboxylate anion, which is a hard Lewis base. Such a difference in the coordination capability between Fe and Co may contribute to the lower Co/Fe ratio incorporated in the framework compared to that in the starting materials. All these results support that, adding Co to this MOF structure at a 1:1 Fe: Co ratio does not affect the final morphology of MIL-88, and yields a stable MOF structure containing a certain level of Co. Further increase of the Co content in the bimetallic MOF turned out to greatly reduce the MOF stability.

The as-synthesized Fe/Co-MIL-88(NH₂) was initially distributed in DMF, the organic solvent used for synthesis. It was reported previously that, exchanging the high boiling point solvent DMF with a lower boiling point solvent like ethanol at elevated temperatures could release the DMF and free ligands resided in the stagnant pore space for the Fe- and MIL-based MOF.^{56, 57} This process is called activation, and can enhance the access to the permanent porosity and increase the surface area of the MOF, which should promote H₂O₂ adsorption to result in higher catalytic activity. Thus, all of the MOF materials used in the following assays were treated by hot ethanol and dried in vacuum. The size distribution profile and the PXRD spectrum of the MOF were highly similar

before and after activation (**Figure S2**), confirming that activation did not break or alter the coordination framework. Notably, the resultant MOF was very stable during dry storage: the DSL (**Figure S3**) and PXRD (**Figure S4**) results of Fe/Co-MIL-88(NH₂) stored for 1 or 3 weeks at room temperature were the same as the freshly synthesized sample.

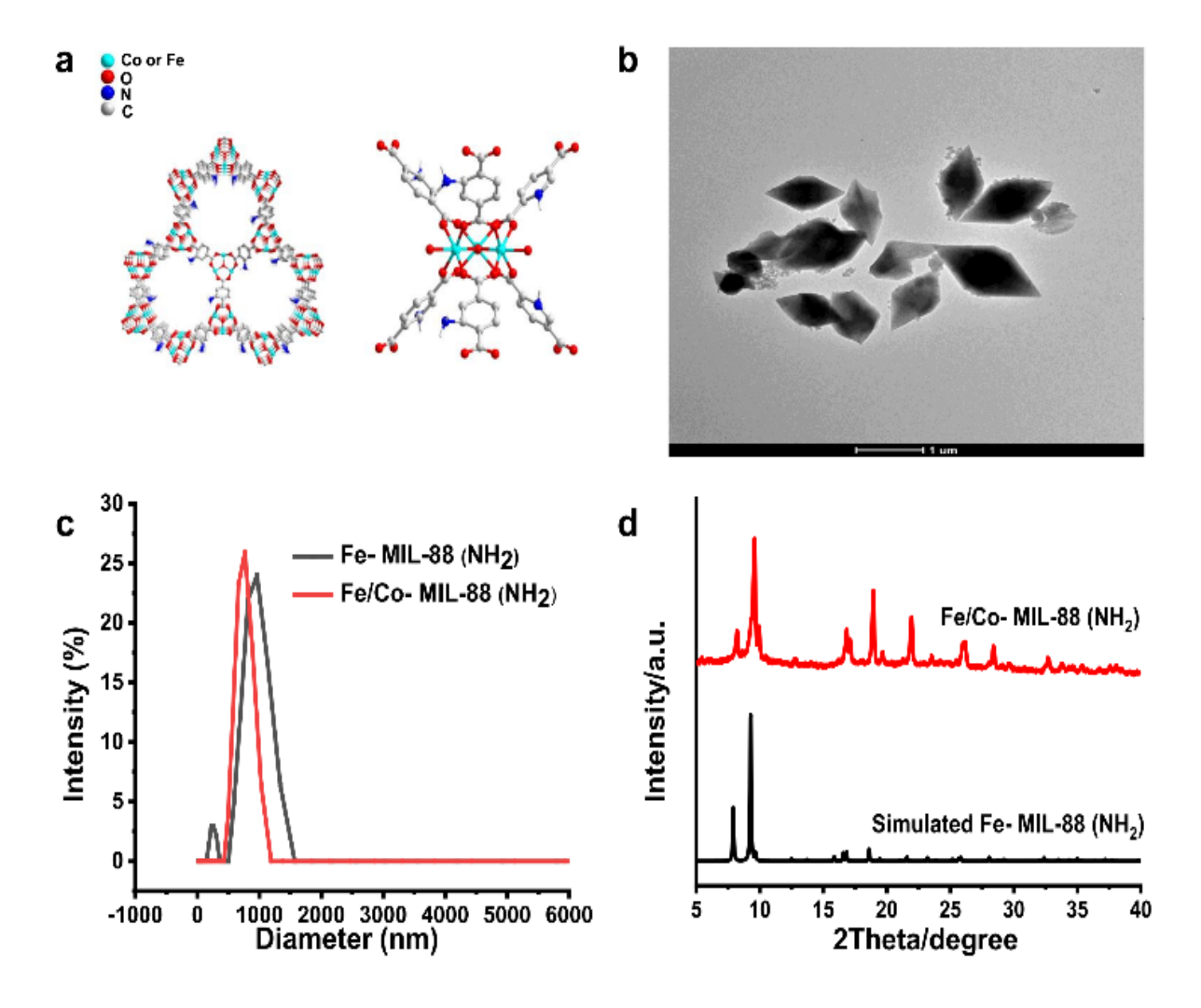


Figure 1. MOF characterization. a) Structure schematic diagram and b) TEM image of Fe/Co-MIL-88(NH₂); c) DSL and d) powder XRD results for simulated Fe- MIL-88(NH₂) and synthesized Fe/Co-MIL-88(NH₂).

Peroxidase-like Activity of Fe/Co-MIL-88(NH₂). We evaluated the peroxidase-like activities of Fe/Co-MIL-88(NH₂) MOF using the model reaction, i.e. the oxidation of the colorless TMB into the blue oxTMB by H_2O_2 (Figure 2a).³⁸ As seen from Fig. 2b, the characteristic, visible light absorption at 652 nm for oxTMB was observed when mixing 25 µg/mL Fe/Co-MIL-88(NH₂) with 1.0 mM H_2O_2 and 1.0 mM TMB in 200 mM NaAc-HAc buffer at pH 4.1. In contrast, the absorbance value was close 0 with only the MOF and H_2O_2 , or with only the TMB and H_2O_2 . These results point out that the bimetallic MOF could act like a peroxidase to catalyze reactions with H_2O_2 . However, a small increase in absorbance observed by mixing the MOF with TMB indicates the existence of a low level of the oxidase-like activity, but the peak intensity was ~ 6.1 folds smaller than that generated by the reaction with MOF and H_2O_2 . Low oxidase-like activity has also been reported in other Fe-based MOF materials.⁵⁸

We also compared the catalytic activity of the pure Fe-based MIL-88(NH₂) MOF with that of the bimetallic one, both MOF materials going through the activation procedure. Using the same amount (5.0 μ g) of the MOF crystals, Fe/Co-MIL-88(NH₂) indeed resulted in ~ 2.5-fold faster increase in absorbance along with increasing H₂O₂ concentrations than Fe-MIL-88(NH₂) (**Fig. 2c**). At the highest H₂O₂ concentration tested, i.e. 1 mM, the bimetallic MOF produced a signal ~2.1 times higher. This result illustrates that, introduction of Co(II) does enhance the catalytic capability of the Fe-based MIL-88(NH₂). It is worth noting that, without "activation", the bimetallic MOF resulted in a signal increase with increasing H₂O₂ concentrations ~3.5-fold slower than that obtained with the activated version (**Figure S5**), probably due to the lower access to the permanent pore surfaces with the trapped DMF solvent.



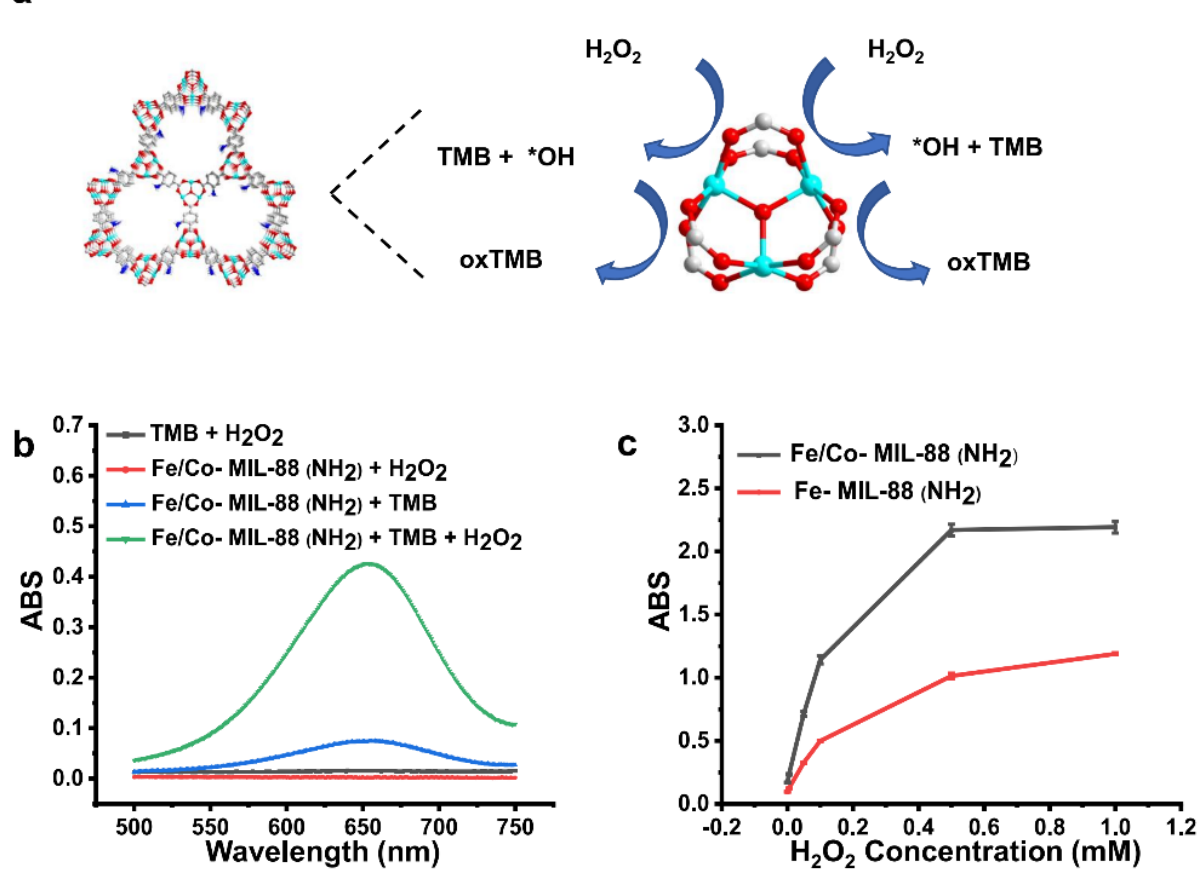


Figure 2. Peroxidase-like activity of Fe/Co-MIL-88(NH₂). a) Schematic illustration of the reaction between TMB and H_2O_2 catalyzed by MOF. b) UV-Vis absorption spectra of the 200- μ L mixture of 1.0 mM TMB and 1.0 mM H_2O_2 with or without 25 ug/ml MOF, and the two control reactions of mixing the MOF with TMB or H_2O_2 only. All reactions measured at 5 min. c) Absorbance (at λ = 652 nm) of oxTMB produced by the 15-min reaction of 1 mM TMB and various H_2O_2 concentrations catalyzed by 50 μ g/ml Fe-MIL-88(NH₂) or Fe/Co-MIL-88(NH₂). All reactions took place in 200 mM NaAc-HAc buffer at pH 4.1.

Steady-State Kinetics Analysis. More detailed assessment of the catalytic capability of the bimetallic MOF was carried out by the steady-state kinetic analysis. The absorbance change at

concentrations. The initial production rate (V in μ M.min⁻¹) of oxTMB within the first 15-min of the reaction window (**Figure 3a**) was plotted against the H₂O₂ concentrations ([S]) to yield the Michaelis-Menten curve (**Figure 3b**). Rearranging **Fig. 3b** to the Lineweaver-Burk plot (**Figure S6**) can attain the Michaelis constant (K_m) and maximum reaction velocity (V_{max}) from the slope and Y-intercept of this linear regression curve: $[1/V = (K_m/V_{max}) \times (1/[S]) + 1/V_{max}]$. The catalytic constant (k_{cat}) can be obtained by dividing the V_{max} by the molar concentration of the "enzyme", the bimetallic Fe/Co-MIL-88(NH₂), which was calculated by counting the number of individual crystal dispersed in a solution of 10 μ L under an optical microscope. The K_m and k_{cat} against the other substrate, TMB, was also measured (**Figure S7**). K_m indicates the binding affinity between the substrate and the enzyme, a smaller value representing a higher affinity. A high value of k_{cat} corresponds to a fast signal generation speed achievable per unit concentration of the enzyme.

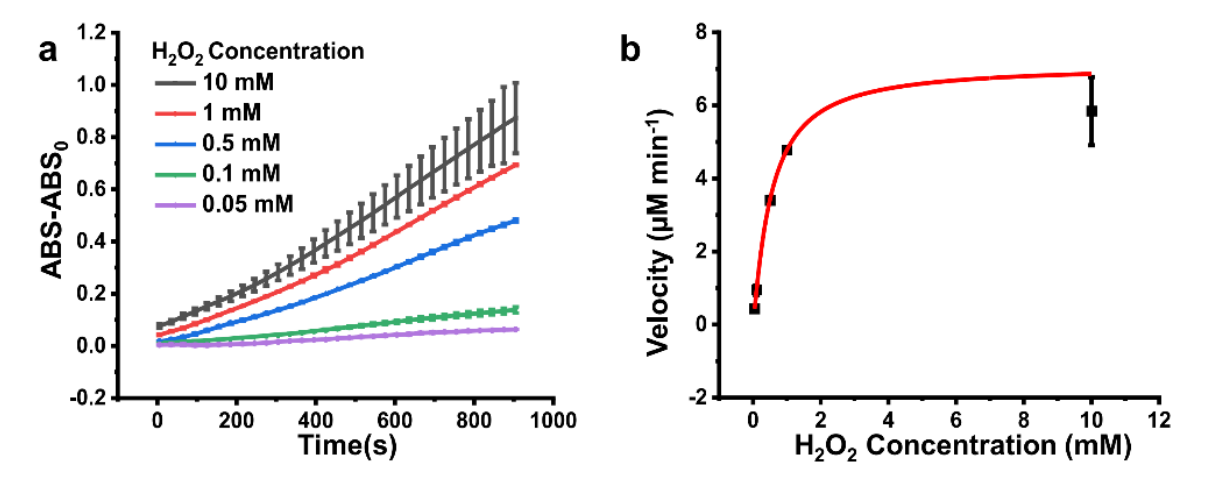


Figure 3. Steady-state kinetics study. a) Increase of absorbance at $\lambda = 652$ nm between 0 and 900 seconds after mixing 1.0 mM TMB, 50 µg/mL Fe/Co-MIL-88(NH₂), and 0.050 – 10 mM H₂O₂. b) Plotting the initial reaction velocity calculated from the absorbance change shown in a) against the corresponding H₂O₂ concentrations. All reactions were in 200 mM NaAc-HAc buffer at pH 4.1.

A K_m of 0.71 mM was found for Fe/Co-MIL-88(NH₂) to H₂O₂, smaller than that of the HRP and most of the MOF-based HRP mimics reported in literature (**Table 1**). In addition, the k_{cat} of Fe/Co-MIL-88(NH₂) measured with varying H₂O₂ concentrations were 3.8 × 10⁴ s⁻¹, much larger than those of HRP. Similarly, the K_m and k_{cat} values related to TMB were also more optimal than the reported values. In particular, compared to the monometallic Fe-MIL-88 (NH₂), the bimetallic MOF has higher affinities to both TMB and H₂O₂, and higher values of k_{cat} . The high enzymatic activity could be owing to the highly porous MOF structure and the exposed metal sites on the MOF surface that strongly facilitate the binding and reaction with H₂O₂. Addition of the more active metal of Co also helps enhance the peroxidase-like activity of the Fe-based MOF. On the other hand, the high k_{cat} constant obtained from the bimetallic MOF we prepared could be attributed to its much larger average size (~ 700 – 1,100 nm in length × ~ 500 nm in diameter) compared to the MOF materials reported in **Table 1** (dimensions ranging from 80 nm to 200 nm): a larger crystal contains more metals than a smaller one per crystal, and thus more active sites.

Table 1. Comparison of the catalytic parameters of HRP and HRP-mimicking MOFs.

Enzyme or Enzyme Mimicking MOF	Substrate	K _m [mM]	k _{cat} [S ⁻¹]	Ref
HRP	TMB	0.43	4.0*10 ³	59
	H_2O_2	3.7	3.5*10 ³	
Co-Ferrocene MOF	TMB	-	-	60
	H_2O_2	28	-	
Copper hexacyanoferrate	TMB	-	-	61
	H_2O_2	72	-	
COF-MOF hybrid	TMB	0.29	14	
	H ₂ O ₂	0.46	10	62
NH ₂ -MIL-88B (Fe)	TMB	1.0	5.0	
	H_2O_2	0.91	3.0	
Fe/Co-MIL-88 (NH ₂)	TMB	0.16	1.1*10 ⁴	This work
	H_2O_2	0.71	3.8 *104	

Bimetallic Fe/Co-MIL-88 (NH₂) as HRP-mimic for signal amplification via a cascade enzymatic reaction. The high peroxidase-mimicking activity possessed by Fe/Co-MIL-88 (NH₂) supports the feasibility that it can be exploited to detect the trace amounts of biomarkers like EVs in clinical samples for disease diagnosis and prognosis. Among different EV classes, exosomes derived from endosomes have attracted great attention in biomarker study, because their unique biogenesis pathways make them carry the molecular composition originated from their parent cells and reflective to the complex physiological states of the cell of origin. ⁶³ We designed the detection assay that starts with using the MOF to isolate the target exosomes from samples and then employs the cascade enzymatic reaction for signal generation (Figure 4a), taking advantage of both the high peroxidase-like activity. The large physical size of the MOF is suitable for exosome isolation from samples for enrichment and purification before detection, because it can be rapidly centrifuged down and removed from solutions. Since multiple surface proteins could present on the surface of each exosome captured by the MOF, they could bind to multiple copies of the GOxlabeled antibodies to catalyze the reaction between glucose and oxygen and generate H₂O₂, the substrate for the peroxidase-like MOF. Like in the enzyme activity measurements mentioned above, TMB can be oxidized and the signal of oxTMB can be used to quantify the target exosomes in samples.

We first tested the feasibility of the cascade enzymatic reaction by conjugating the GOx with biotin and the MOF with streptavidin. Pulling down the biotinylated GOx by the streptavidin-conjugated MOF produced the blue oxTMB in 200 mM acetate buffer (pH 4.1), when supplied with glucose and TMB. We also explored the conditions of the detection platform, and found that, 6.0 mg MOF yielded a relatively higher change in the absorbance signal from oxTMB than 3.0 and 0.30 mg (**Figure S8**). In consideration of keeping material consumption low, we chose to use

3.0 mg in the following experiments. We also found that, among the different glucose (0.50, 1.0, 2.0, 15 mM) and TMB (0.50, 1.0, and 1.5 mM) concentrations tested, the lowest concentrations led to the largest signal to background ratio (**Figure S8**), because higher substrate concentrations significantly increased the background signal with low GOx concentrations. We speculate that, with a high glucose concentration, the speed of H₂O₂ generation may exceed that of H₂O₂ decomposition. The accumulated H₂O₂ could oxidize TMB to result in high background. Under the optimal reaction condition, i.e. using 3.0 mg MOF, 0.50 mM glucose and 0.50 mM TMB, as low as 0.17 nM GOx could be detected (**Fig. S8**).

Next, we employed the bimetallic MOF to detect exosomes in biological samples. Since CD63 is a specific tetraspanin marker displayed on exosome surface, we labeled the bimetallic MOF with the anti-CD63 aptamer for exosome capture, using glutaraldehyde as the crosslinker. Glutaraldehyde firstly reacted with the –NH2 groups on the surface of the bimetallic MOF, and then linked with the NH2-modified aptamer (Figure S9a). The residual reactive glutaraldehyde was quenched by 0.1 M glycine, and the MOF surface was further covered by polyethylene glycol (PEG) through physical adsorption to prevent non-specific binding. Size measurement by DLS displayed comparable size distribution profiles of the Fe/Co-MIL-88(NH2) with or without glutaraldehyde modification (Figure S9b). However, aptamer conjugation caused ~23% reduction of the signal-to-noise ratio generated from the MOF-catalyzed TMB oxidation, while further surface passivation with PEG had little effect on the peroxidase activity of MOF (Figure S9c). Substrate access to the open metal site on MOF surface may be impeded by the conjugated aptamer and ad adsorbed PEG. Aptamer could also increase the negative charges on the MOF surface that may reduce the affinity of the electron-rich substrates of TMB and H₂O₂.

Then the biotinylated anti-CD9 was employed to bind to another specific tetraspanin marker for exosome, CD9, on exosome surface. We chose to use streptavidin to bridge the biotinylated GOx on the MOF and the biotinylated anti-CD9 on exosome. In this way, the detection antibody or GOx was conjugated with the small biotin tag that imposes negligible impedance to their biological activities. In addition, we expect the multiple layers of the biotin-streptavidin assembly may help immobilize more GOx on each MOF surface through attachment of exosomes, which could be at limited amounts in biological samples. Using the standard exosomes purchased from a commercial supplier and 3.0 mg MOF, we confirmed that the cascade enzymatic reaction using GOx and peroxidase-mimicking MOF can detect exosomes dispersed in 1× PBS at concentrations ranging from 1.6×10^5 - 1.6×10^6 particles/mL (P/mL) (Figure 4b). The limit of detection (LOD) was calculated to be 7.8×10^4 P/mL with the 3σ method. Such a detection range is lower than that obtained by NTA (10^8 – 10^9 P/mL) and the HRP-based ELISA (between $10^6 \sim 10^8$ P/mL) (Figure S10).^{64,65}

Exosome detection in biological samples. With the superior detection performance demonstrated for the bimetallic MOF, we applied the assay to detect exosomes in cell culture medium and human serum. We harvested the exosomes in the culture medium of HeLa cells for 12, 24, and 48 hrs, and took 1 μL of the harvested EVs to be analyzed by the aptamer-conjugated bimetallic MOF. The harvested EVs were diluted 15,000 times and 20 μL of the dilution was used in the assay. We clearly observed that the blue color of the detection solution turned darker with longer harvest times and the absorbance increase was significantly different between different time points (Fig. 4c). This result supports that our assay can be used to monitor exosome production from cell lines, which could be stimulated to increase or reduce vesicle productions for exosome biogenesis study. The large dilution factor we used for this harvested EV sample illustrates the

possibility of direct sampling of the cell culture medium for monitoring of EV production by cells by our assay, avoiding the tedious steps of ultracentrifugation.

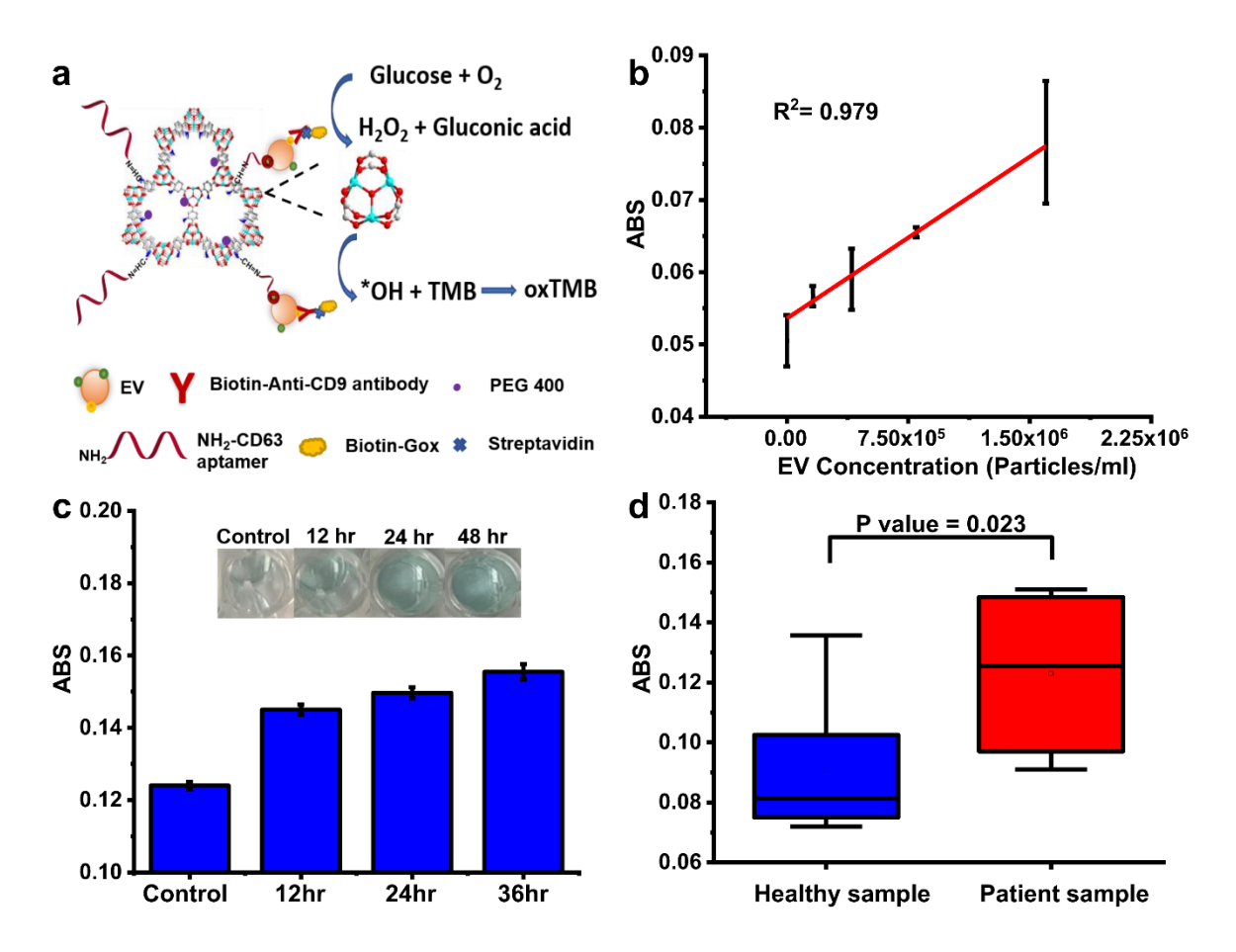


Figure 4. Application of Fe/Co-MIL-88(NH₂) for EV detection. a) Scheme of EV detection facilitated by the cascade reaction between the peroxidase-mimicking Fe/Co-MIL-88(NH₂) and GOx. b) Calibration curve of the assay for detection EVs dispersed in 1× PBS. c) Colorimetric signal resulted from detection of EVs secreted by HeLa cells at various time points. d) Detection of EVs in the sera samples from healthy controls (n=8) and breast cancer patients (n=8). The detection solution contained 0.50 mM TMB, 3.0 mg MOF, and 0.50 mM glucose, in 200 mM NaAc-HAc buffer at pH 4.1.

Moreover, we detected exosomes in serum samples collected from breast cancer patients and healthy people (n = 8 for each cohort). We found that the exosome concentrations in these clinical samples were much higher than the upper detection limit of our assay, and $10,000 \times$ dilution was needed for all samples. This means that we only needed far less than 1 μ L serum for each measurement. The exosome concentrations were found significantly higher (p < 0.05) in patients' sera samples (**Fig. 4d**) than that found in the samples of healthy controls. The bimetallic MOF can enable sensitive exosome detection in complex biological matrices with ultra-low sample consumption, proving its high potential in clinical applications.

CONCLUSION

In the present work, we report a bimetallic Fe/Co-MIL-88(NH₂) with superior peroxidase catalytic activities and good stability, and evaluate its peroxidase-like activity. Because of the abundant active site and synergistic effect between Fe and Co, the Fe/Co-MIL-88(NH₂) exhibits superior catalytic activity to HRP and the monometallic Fe-MIL-88(NH₂). It can also enable sensitive exosome detection while forming a cascade reaction with GOx, demonstrating great potential to be signaling labels in bioassays for detection of biomarkers. We believe that the design of including multiple metals in one MOF structure could produce more MOFs with superior enzyme-like characteristics and expand the collection of nanozymes for broader scopes of applications.⁶⁶⁻⁶⁸

Some improvements are still needed to further move forward clinical applications of this peroxidase-like MOF material. For example, the dynamic range is quite narrow in the current format. The intrinsic oxidase activity towards TMB of the bimetallic MOF produces a high background at low target concentrations: with a low target concentration, only a very low amount

of GOx could be immobilized on the MOF and generate a very low amount of H₂O₂, being

outcompeted by O₂ in the air to produce oxTMB. On the other hand, with a high target

concentration, the colorimetric signal would drop significantly, probably because the H₂O₂

concentration is too high and at very close proximity to the MOF that would destroy the MOF

structure and prevent further signal increase. Both factors contribute to a narrow detection dynamic

range by the cascade enzymatic reaction scheme. Other signaling strategies and MOF designs

could be adopted to improve the detection range in future studies.

ASSOCIATED CONTENT

Supporting Information

Additional data of material characterization, catalytic activity comparison, steady-state kinetic

measurement; assay optimization and performance comparison with ELISA; and clinical sample

information. This material is available free of charge via the Internet at http://pubs.acs.org.

AUTHOR INFORMATION

Corresponding Author

* E-mail: pingyun.feng@ucr.edu; wenwan.zhong@ucr.edu

ACKNOWLEDGMENTS

The authors would like to thank the National Science Foundation (CHE-1707347 to W.Z.) for

funding and we also acknowledge the support of the MOF synthesis and characterization by the

US Department of Energy, Office of Basic Energy Sciences, Materials Sciences and Engineering

Division under Award No. DE-SC0010596 (P.F.).

REFERENCE

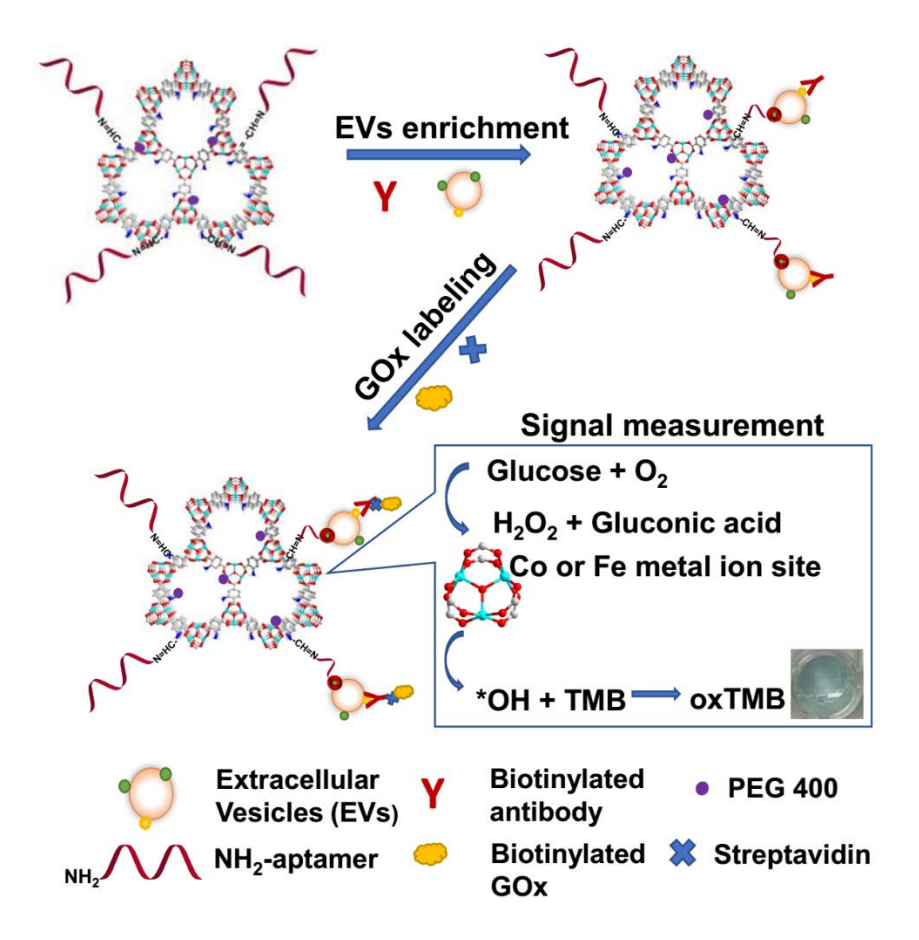
- (1) Lu, K.; Aung, T.; Guo, N.; Weichselbaum, R.; Lin, W. Nanoscale Metal-Organic Frameworks for Therapeutic, Imaging, and Sensing Applications. *Adv. Mater.* **2018**, *30*, 1707634.
- (2) Yang, H.; Wang, Y.; Krishna, R.; Jia, X.; Wang, Y.; Hong, A. N.; Dang, C.; Castillo, H. E.; Bu, X.; Feng, P. Pore-Space-Partition-Enabled Exceptional Ethane Uptake and Ethane-Selective Ethane-Ethylene Separation. *J. Am. Chem. Soc.* **2020**, *142*, 2222–2227.
- (3) Hong, A. N.; Yang, H.; Li, T.; Wang, Y.; Wang, Y.; Jia, X.; Zhou, A.; Kusumoputro, E.; Li, J.; Bu, X.; Feng, P. Pore-Space Partition and Optimization for Propane-Selective High-Performance Propane/Propylene Separation. *ACS Appl. Mater. Interfaces.* **2021**, *13*, 52160–52166.
- (4) Lu, X. F.; Fang, Y.; Luan, D.; Lou, X. W. Metal-Organic Frameworks Derived Functional Materials for Electrochemical Energy Storage and Conversion: A Mini Review. *Nano Lett.* **2021**, 21, 1555–1565.
- (5) Indra, A.; Song, T.; Paik, U. Metal Organic Framework Derived Materials: Progress and Prospects for the Energy Conversion and Storage. *Adv. Mater.* **2018**, *30*, 1705146.
- (6) Xu, W.; Jiao, L.; Wu, Y.; Hu, L.; Gu, W.; Zhu, C. Metal-Organic Frameworks Enhance Biomimetic Cascade Catalysis for Biosensing. *Adv. Mater.* **2021**, *33*, 2005172.
- (7) Rasheed, T.; Rizwan, K. Metal-Organic Frameworks Based Hybrid Nanocomposites as State-of-the-Art Analytical Tools for Electrochemical Sensing Applications. *Biosens. Bioelectron.* **2022**, *199*, 113867.
- (8) Zhang, X.; Lin, S.; Liu, S.; Tan, X.; Dai, Y.; Xia, F. Advances in Organometallic/Organic Nanozymes and Their Applications. *Coord. Chem. Rev.* **2021**, *429*, 213652.
- (9) Ji, S.; Jiang, B.; Hao, H.; Chen, Y.; Dong, J.; Mao, Y.; Zhang, Z.; Gao, R.; Chen, W.; Zhang, R; Liang, Q. Matching the Kinetics of Natural Enzymes with a Single-Atom Iron Nanozyme. *Nat. Catal.* **2021**, *4*1, 407–417.
- (10) Wang, S.; Zhao, Y.; Wang, M.; Li, H.; Saqib, M.; Ge, C.; Zhang, X.; Jin, Y. Enhancing Luminol Electrochemiluminescence by Combined Use of Cobalt-Based Metal Organic Frameworks and Silver Nanoparticles and Its Application in Ultrasensitive Detection of Cardiac Troponin I. *Anal. Chem.* **2019**, *91*, 3048–3054.
- (11) Shao, K.; Wang, B.; Nie, A.; Ye, S.; Ma, J.; Li, Z.; Lv, Z.; Han, H. Target-Sriggered Signal-on Ratiometric Electrochemiluminescence Sensing of PSA Based on MOF/Au/G-Quadruplex. *Biosens. Bioelectron.* **2018**, *118*, 160–166.
- (12) Wang, Z.; Jiang, X.; Yuan, R.; Chai, Y. N-(Aminobutyl)-N-(Ethylisoluminol) Functionalized Fe-Based Metal-Organic Frameworks with Intrinsic Mimic Peroxidase Activity for Sensitive Electrochemiluminescence Mucin1 Determination. *Biosens. Bioelectron.* **2018**, *121*, 250–256.
- (13) Zhao, X.; Zhang, N.; Yang, T.; Liu, D.; Jing, X.; Wang, D.; Yang, Z.; Xie, Y.; Meng, L. Bimetallic Metal–Organic Frameworks: Enhanced Peroxidase-like Activities for the Self-Activated Cascade Reaction. *ACS Appl. Mater. Interfaces.* **2021**, *13*, 36106–36116.
- (14) Zhang, Y.; Feng, Y.-S.; Ren, X.-H.; He, X.-W.; Li, W.-Y.; Zhang, Y.-K. Bimetallic Molecularly Imprinted Nanozyme: Dual-Mode Detection Platform. *Biosens. Bioelectron.* **2022**, *196*, 113718.
- (15) Huang, Y.; Ren, J.; Qu, X. Nanozymes: Classification, Catalytic Mechanisms, Activity Regulation, and Applications. *Chem. Rev.* **2019**, *119*, 4357–4412.

- (16) Niu, X.; Li, X.; Lyu, Z.; Pan, J.; Ding, S.; Ruan, X.; Zhu, W.; Du, D.; Lin, Y. Metal-Organic Framework Based Nanozymes: Promising Materials for Biochemical Analysis. *Chem. Commun.* **2020,** *56*, 11338–11353.
- (17) He, L.; Li, Y.; Wu, Q.; Wang, D. M.; Li, C. M.; Huang, C. Z.; Li, Y. F. Ru (III)-Based Metal-Organic Gels: Intrinsic Horseradish and NADH Peroxidase-Mimicking Nanozyme. *ACS Appl. Mater. Interfaces.* **2019**, *11*, 29158–29166.
- (18) Iraci, N.; Leonardi, T.; Gessler, F.; Vega, B.; Pluchino, S. Focus on Extracellular Vesicles: Physiological Role and Signalling Properties of Extracellular Membrane Vesicles. *Int. J. Mol. Sci.* **2016**, *17*, 171/1–171/32.
- (19) Kraemer-Albers, E.-M.; Hill, A. F. Extracellular Vesicles: Interneural Shuttles of Complex Messages. *Curr. Opin. Neurobio.* **2016**, *39*, 101–107.
- (20) Shifrin, D. A., Jr.; Beckler, M. D.; Coffey, R. J.; Tyska, M. J. Extracellular Vesicles: Communication, Coercion, and Conditioning. *Mol. Biol. Cell.* **2013**, *24*, 1253–1259.
- (21) Turturici, G.; Tinnirello, R.; Sconzo, G.; Geraci, F. Extracellular Membrane Vesicles as a Mechanism of Cell-to-Cell Communication: Advantages and Disadvantages. *Am. J. Physiol. Cell Physiol.* **2014**, *306*, C621–C633.
- (22) Yanez-Mo, M.; Siljander, P. R. M.; Andreu, Z.; Zavec, A. B.; Borras, F. E.; Buzas, E. I.; Buzas, K.; Casal, E.; Cappello, F.; Carvalho, J.; Colas, E.; Cordeiro-da Silva, A.; Fais, S.; Falcon-Perez, J. M.; Ghobrial, I. M.; Giebel, B.; Gimona, M.; Graner, M.; Gursel, I.; Gursel, M.; Heegaard, N. H. H.; Hendrix, A.; Kierulf, P.; Kokubun, K.; Kosanovic, M.; Kralj-Iglic, V.; Kramer-Albers, E.-M.; Laitinen, S.; Lasser, C.; Lener, T.; Ligeti, E.; Line, A.; Lipps, G.; Llorente, A.; Lotvall, J.; Mancek-Keber, M.; Marcilla, A.; Mittelbrunn, M.; Nazarenko, I.; Nolte-'t Hoen, E. N. M.; Nyman, T. A.; O'Driscoll, L.; Olivan, M.; Oliveira, C.; Pallinger, E.; Del Portillo, H. A.; Reventos, J.; Rigau, M.; Rohde, E.; Sammar, M.; Sanchez-Madrid, F.; Santarem, N.; Schallmoser, K.; Ostenfeld, M. S.; Stoorvogel, W.; Stukelj, R.; Van der Grein, S. G.; Vasconcelos, M. H.; Wauben, M. H. M.; De Wever, O. Biological Properties of Extracellular Vesicles and Their Physiological Functions. *J. Extracell. Vesicles.* **2015**, *4*, 27066–27066.
- (23) Crowley, E.; Di Nicolantonio, F.; Loupakis, F.; Bardelli, A. Liquid Biopsy: Monitoring Cancer-Genetics in the Blood. *Nat. Rev. Clin. Oncol.* **2013**, *10*, 472–484.
- (24) Lo Cicero, A.; Stahl, P. D.; Raposo, G. Extracellular Vesicles Shuffling Intercellular Messages: for Good or for Bad. *Curr. Opin. Cell Biol.* **2015**, *35*, 69–77.
- (25) Atayde, V. D.; Hassani, K.; da Silva Lira Filho, A.; Borges, A. R.; Adhikari, A.; Martel, C.; Olivier, M. Leishmania Exosomes and Other Virulence Factors: Impact on Innate Immune Response and Macrophage Functions. *Cell. Immunol.* **2016**, *309*, 7–18.
- (26) Broekman, M. L.; Maas, S. L. N.; Abels, E. R.; Mempel, T. R.; Krichevsky, A. M.; Breakefield, X. O. Multidimensional Communication in the Microenvirons of Glioblastoma. *Nat. Rev. Neurol.* **2018**, *14*, 482–495.
- (27) Guo, Y.; Ji, X.; Liu, J.; Fan, D.; Zhou, Q.; Chen, C.; Wang, W.; Wang, G.; Wang, H.; Yuan, W.; Ji, Z.; Sun, Z. Effects of Exosomes on Pre-Metastatic Niche Formation in Tumors. *Mol. Cancer.* **2019**, *18*, 39.
- (28) Schorey, J. S.; Cheng, Y.; Singh, P. P.; Smith, V. L. Exosomes and Other Extracellular Vesicles in Host-Pathogen Interactions. *EMBO Rep.* **2015**, *16* (1), 24–43.
- (29) Zhang, P.; Zhou, X.; Zeng, Y. Multiplexed Immunophenotyping of Circulating Exosomes on Nano-Engineered ExoProfile Chip Towards Early Diagnosis of Cancer. *Chem. Sci.* **2019**, *10*, 5495–5504.

- (30) Li, A.; Zhang, T.; Zheng, M.; Liu, Y.; Chen, Z. Exosomal Proteins as Potential Markers of Tumor Diagnosis. *J. Hematol. Oncol. Pharm.* **2017**, *10*, 1–9.
- (31) Huang, G.; Lin, G.; Zhu, Y.; Duand, W.; Jin, D. Emerging Technologies for Profiling Extracellular Vesicle Heterogeneity. *Lab on a Chip.* **2020**, *20*, 2423.
- (32) Min, J.; Son, T.; Hong, J.-S.; Cheah, P. S.; Wegemann, A.; Murlidharan, K.; Weissleder, R.; Lee, H.; Im, H. Plasmon-Enhanced Biosensing for Multiplexed Profiling of Extracellular Vesicles. *Adv. Biosys.* **2020**, 2000003.
- (33) Wu, D.; Yan, J.; Shen, X.; Sun, Y.; Thulin, M.; Cai, Y.; Wik, L.; Shen, Q.; Oelrich, J.; Qian, X.; Dubois, K. L.; Ronquist, K. G.; Nilsson, M.; Landegren, U.; Kamali-Moghaddam, M. Profiling Surface Proteins on Individual Exosomes Using a Proximity Barcoding Assay. *Nat. Commun.* **2019**, *10*, 3854.
- (34) Zhang, P.; Wu, X.; Gardashova, G.; Yang, Y.; Zhang, Y.; Xu, L.; Zeng, Y. Molecular and Functional Extracellular Vesicle Analysis Using Nanopatterned Microchips Monitors Tumor Progression and Metastasis. *Science Translational Medicine*. **2020**, *12* (547), eaaz2878.
- (35) Min, L.; Wang, B.; Bao, H.; Li, X.; Zhao, L.; Meng, J.; Wang, S. Advanced Nanotechnologies for Extracellular Vesicle-Based Liquid Biopsy. *Adv. Sci.* **2021**, *8*, 2102789.
- (36) Abreu, C. M.; Costa-Silva, B.; Reis, R. L.; Kundu, S. C.; Caballero, D. Microfluidic Platforms for Extracellular Vesicle Isolation, Analysis and Therapy in Cancer. *Lab on a Chip.* **2022**, *22*, 1093–1125.
- (37) Wei, Y.-S.; Zhang, M.; Kitta, M.; Liu, Z.; Horike, S.; Xu, Q. A Single-Crystal Open-Capsule Metal-Organic Framework. *J. Am. Chem. Soc.* **2019**, *141*, 7906–7916.
- (38) Jiang, B.; Duan, D.; Gao, L.; Zhou, M.; Fan, K.; Tang, Y.; Xi, J.; Bi, Y.; Tong, Z.; Gao, G. F.; Xie, N.; Tang, A.; Nie, G.; Liang, M.; Yan, X. Standardized Assays for Determining the Catalytic Activity and Kinetics of Peroxidase-Like Nanozymes. *Nat. Protoc.* **2018**, *13*, 1506–1520.
- (39) Liu, B.; Vikrant, K.; Kim, K.-H.; Kumar, V.; Kailasa, S. K. Critical Role of Water Stability in Metal-Organic Frameworks and Advanced Modification Strategies for the Extension of Their Applicability. *Environ. Sci. Nano.* **2020**, *7*, 1319–1347.
- (40) Ma, M.; Noei, H.; Mienert, B.; Niesel, J.; Bill, E.; Muhler, M.; Fischer, R. A.; Wang, Y.; Schatzschneider, U.; Metzler Nolte, N. Iron Metal-Organic Frameworks MIL 88B and NH2 MIL 88B for the Loading and Delivery of the Gasotransmitter Carbon Monoxide. *Eur. J. Chem.* **2013**, *19*, 6785–6790.
- (41) Mo, G.; Qin, D.; Jiang, X.; Zheng, X.; Mo, W.; Deng, B. A Sensitive Electrochemiluminescence Biosensor Based on Metal-Organic Framework and Imprinted Polymer for Squamous Cell Carcinoma Antigen Detection. *Sens. Actuators B Chem.* 2020, 310, 127852.
- (42) Pereira, M.; Oliveira, L.; Murad, E. Iron Oxide Catalysts: Fenton and Fentonlike Reactions-a Review. *Clay minerals.* **2012**, *47*, 285–302.
- (43) Li, J.; Chu, D.; Dong, H.; Baker, D. R.; Jiang, R. J. Boosted Oxygen Evolution Reactivity by Igniting Double Exchange Interaction in Spinel Oxides. *J. Am. Chem. Soc.* **2019**, *142*, 50–54.
- (44) Gao, C.; Chen, S.; Quan, X.; Yu, H.; Zhang, Y. Enhanced Fenton-Like Catalysis by Iron-Based Metal Organic Frameworks for Degradation of Organic Pollutants. *J. Catal.* **2017**, *356*, 125–132.
- (45) Yang, X.-j.; Xu, X.-m.; Xu, J.; Han, Y. Iron Oxychloride (FeOCl): an Efficient Fenton-Like Catalyst for Producing Hydroxyl Radicals in Degradation of Organic Contaminants. *J. Am. Chem. Soc.* **2013**, *135*, 16058–16061.

- (46) Zhou, W.; Gao, J.; Zhao, H.; Meng, X.; Wu, S. The Role of Quinone Cycle in Fe^{2+} - H_2O_2 System in the Regeneration of Fe^{2+} . *Environ. Technol.* **2017**, *38*, 1887–1896.
- (47) Spier, E.; Neuenschwander, U.; Hermans, I. Insights into the Cobalt (II) Catalyzed Decomposition of Peroxide. *Angew. Chem. Int. Ed.* **2013**, *52*, 1581–1585.
- (48) Leonard, S.; Gannett, P. M.; Rojanasakul, Y.; Schwegler-Berry, D.; Castranova, V.; Vallyathan, V.; Shi, X. Cobalt-Mediated Generation of Reactive Oxygen Species and Its Possible Mechanism. *J. Inorg. Biochem.* **1998**, *70*, 239–244.
- (49) Dong, H.; Fan, Y.; Zhang, W.; Gu, N.; Zhang, Y. Catalytic Mechanisms of Nanozymes and Their Applications in Biomedicine. *Bioconjugate Chem.* **2019**, *30*, 1273–1296.
- (50) Z Zhou, X.; Fan, C.; Tian, Q.; Han, C.; Yin, Z.; Dong, Z.; Bi, S. Trimetallic AUPTCO Nanopolyhedrons with Peroxidase- and Catalase-Like Catalytic Activity for Glow-Type Chemiluminescence Bioanalysis. *Anal. Chem.* 2021, 94, 847–855.
- (51) Lu, W.; Yuan, M.; Chen, J.; Zhang, J.; Kong, L.; Feng, Z.; Ma, X.; Su, J.; Zhan, J. Synergistic Lewis Acid-Base Sites of Ultrathin Porous Co₃O₄ Nanosheets with Enhanced Peroxidase-Like Activity. *Nano Res.* **2021**, *14*, 3514–3522.
- (52) Jiang, Z.-J.; Cheng, S.; Rong, H.; Jiang, Z.; Huang, J. General Synthesis of MFe₂ O₄/Carbon (M= Zn, Mn, Co, Ni) Spindles From Mixed Metal Organic Frameworks as High Performance Anodes for Lithium Ion Batteries. *J. Mater. Chem.* **2017**, *5*, 23641–23650.
- (53) McKinlay, A. C.; Eubank, J. F.; Wuttke, S.; Xiao, B.; Wheatley, P. S.; Bazin, P.; Lavalley, J. C.; Daturi, M.; Vimont, A.; De Weireld, G.; Horcajada, P.; Serre, C.; Morris, R. E. Nitric Oxide Adsorption and Delivery in Flexible MIL-88(Fe) Metal-Organic Frameworks. *Chem. Mater.* **2013**, *25*, 1592–1599.
- (54) Horcajada, P.; Salles, F.; Wuttke, S.; Devic, T.; Heurtaux, D.; Maurin, G.; Vimont, A.; Daturi, M.; David, O.; Magnier, E.; Stock, N.; Filinchuk, Y.; Popov, D.; Riekel, C.; Férey, G.; Serre, C. How Linker's Modification Controls Swelling Properties of Highly Flexible Iron(III) Dicarboxylates MIL-88. *J. Am. Chem. Soc.* **2011**, *133*, 17839–17847.
- (55) Ramsahye, N. A.; Trung, T. K.; Scott, L.; Nouar, F.; Devic, T.; Horcajada, P.; Magnier, E.; David, O.; Serre, C.; Trens, P. Impact of the Flexible Character of MIL-88 Iron(III) Dicarboxylates on the Adsorption of n-Alkanes. *Chem. Mater.* **2013**, *25*, 479–488.
- (56) Mondloch, J. E.; Karagiaridi, O.; Farha, O. K.; Hupp, J. T. Activation of Metal-Organic Framework Materials. *CrystEngComm.* **2013**, *15*, 9258–9264.
- (57) Otun, K. O. Temperature-Controlled Activation and Characterization of Iron-Based Metal-Organic Frameworks. *Inorganica Chim. Acta.* **2020**, *507*, 119563.
- (58) He, J.; Zhang, Y.; Zhang, X.; Huang, Y. Highly Efficient Fenton and Enzyme-Mimetic Activities of NH2-MIL-88B (Fe) Metal Organic Framework for Methylene Blue Degradation. *Sci. Rep* **2018**, *8*, 1–8.
- (59) Gao, L.; Zhuang, J.; Nie, L.; Zhang, J.; Zhang, Y.; Gu, N.; Wang, T.; Feng, J.; Yang, D.; Perrett, S.; Yan, X. Intrinsic Peroxidase-Like Activity of Ferromagnetic Nanoparticles. *Nat. Nanotechnol.* 2007, 2, 577–583.
- (60) Fang, C.; Deng, Z.; Cao, G.; Chu, Q.; Wu, Y.; Li, X.; Peng, X.; Han, G. Co-Ferrocene MOF/Glucose Oxidase as Cascade Nanozyme for Effective Tumor Therapy. *Adv. Funct. Mater.* **2020**, *30*, 1910085.
- (61) Wang, D.; Wu, H.; Wang, C.; Gu, L.; Chen, H.; Jana, D.; Feng, L.; Liu, J.; Wang, X.; Xu, P.; Guo, Z.; Chen, Q.; Zhao, Y. Self-Assembled Single-Site Nanozyme for Tumor-Specific Amplified Cascade Enzymatic Therapy. *Angew. Chem.* **2021**, *133* (6), 3038–3044.

- (62) Zhang, L.; Liu, Z.; Deng, Q.; Sang, Y.; Dong, K.; Ren, J.; Qu, X. Nature-Inspired Construction of MOF@ COF Nanozyme with Active Sites in Tailored Microenvironment and Pseudopodia-Like Surface for Enhanced Bacterial Inhibition. *Angew. Chem.* **2021**, *60*, 3469–3474. (63) Kalluri, R.; LeBleu, V. S. The Biology, Function, and Biomedical Applications of Exosomes. *Science* **2020**, *367*, eaau6977.
- (64) Zarovni, N.; Corrado, A.; Guazzi, P.; Zocco, D.; Lari, E.; Radano, G.; Muhhina, J.; Fondelli, C.; Gavrilova, J.; Chiesi, A. Integrated Isolation and Quantitative Analysis of Exosome Shuttled Proteins and Nucleic Acids Using Immunocapture Approaches. *Meth.* **2015**, *87*, 46–58.
- (65) Doldán, X.; Fagúndez, P.; Cayota, A.; Laíz, J.; Tosar, J. P. Electrochemical Sandwich Immunosensor for Determination of Exosomes Based on Surface Marker-Mediated Signal Amplification. *Anal. Chem.* **2016**, *88*, 10466–10473.
- (66) Wu, J.; Wang, X.; Wang, Q.; Lou, Z.; Li, S.; Zhu, Y.; Qin, L.; Wei, H. Nanomaterials with Enzyme-Like Characteristics (Nanozymes): Next-Generation Artificial Enzymes (II). *Chem. Soc. Rev.* **2019**, *48* (4), 1004–1076.
- (67) Wei, H.; Wang, E. Nanomaterials with Enzyme-Like Characteristics (Nanozymes): Next-Generation Artificial Enzymes. *Chem. Soc. Rev.* **2013**, *42* (14), 6060–6093.
- (68) Wang, X.; Gao, X. J.; Qin, L.; Wang, C.; Song, L.; Zhou, Y.-N.; Zhu, G.; Cao, W.; Lin, S.; Zhou, L. eg Occupancy as an Effective Descriptor for the Catalytic Activity of Perovskite Oxide-Based Peroxidase Mimics. *Nat. Commun.* **2019**, *10* (1), 1–8.



Supporting Information

Bimetallic Metal-Organic Framework Fe/Co-MIL-88(NH₂) Exhibiting High Peroxidase-like Activity and Its Application in Detection of Extracellular Vesicles

Qiaoshi Jiang,¹ Yuchen Xiao,² Anh N. Hong,² Ziting Gao,² Yuyang Shen,¹ Qingsong Fan,² Pingyun Feng², * and Wenwan Zhong¹,²,*

¹Environmental Toxicology Graduate Program; ²Department of Chemistry, University of California-Riverside,

Riverside, CA 92521

Corresponding Author

* E-mail: pingyun.feng@ucr.edu; wenwan.zhong@ucr.edu

Table of Contents

1. Material Characterization	S-2
2. Material stability investigation	S-3
3. Catalytic activity evaluation	S-4
4. Optimization of the cascade enzyme reaction	S-6
5. Aptamer conjugation and detection comparison with ELISA	S-7

1. Material characterization.

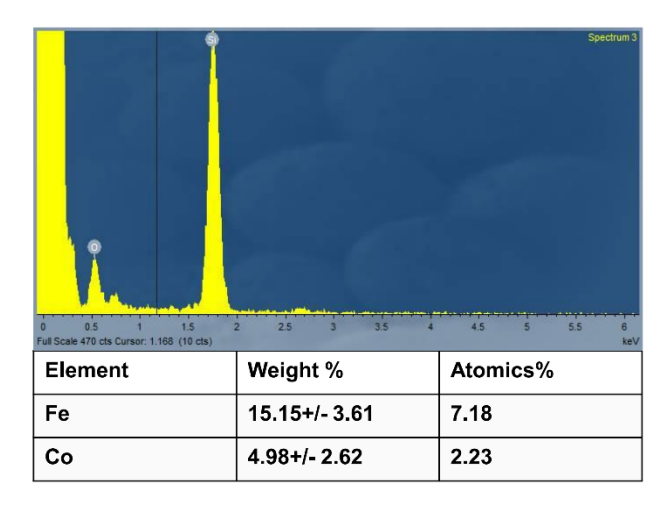


Figure S1. EDS measurement of Fe/Co-MIL-88(NH₂).

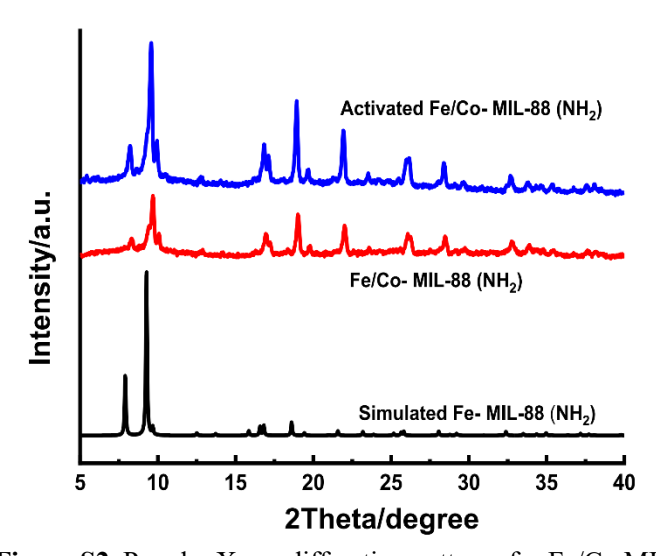


Figure S2. Powder X-ray diffraction patterns for Fe/Co MIL-88(NH₂) before and after activation.

2. Material stability investigation.

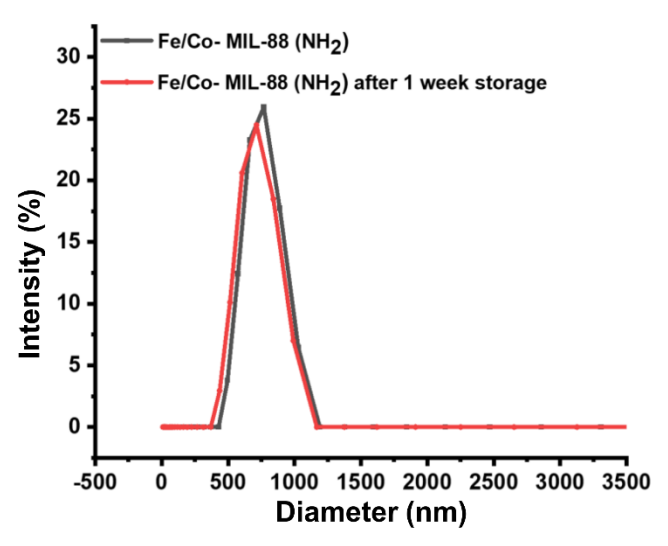


Figure S3. Dynamic Light Scattering results of Fe/Co-MIL-88(NH₂) before and after stored at room temperature for 1 week.

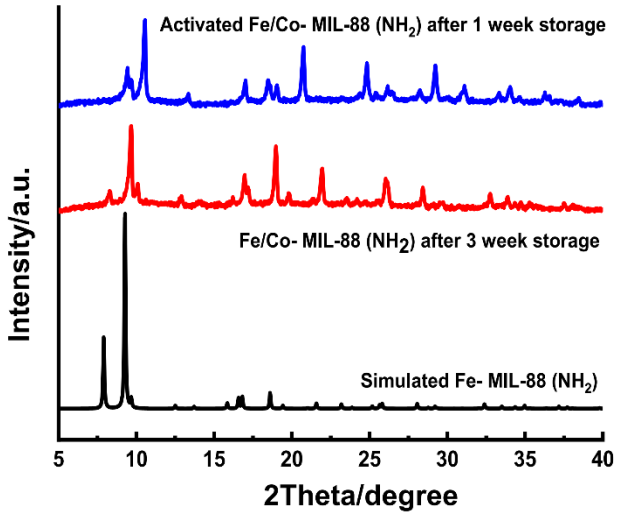


Figure S4. Powder X-ray diffraction results of Fe/Co MIL-88(NH₂) stored at room temperature for 1 and 3 weeks.

3. Catalytic activity evaluation.

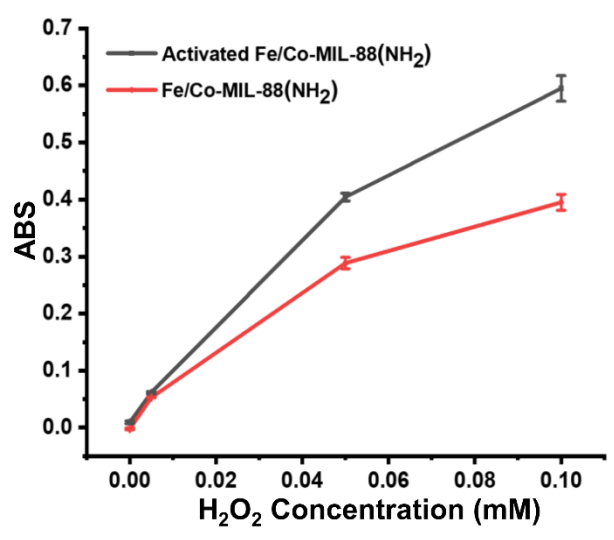


Figure S5. Catalytic ability comparison before and after activation. After activation, more increase of the absorbance signal per unit increase of the H_2O_2 concentration was observed. MOF = 25 μ g/ml in 200 mM NaAc-HAc buffer at pH 4.1. Reaction time = 15 min.

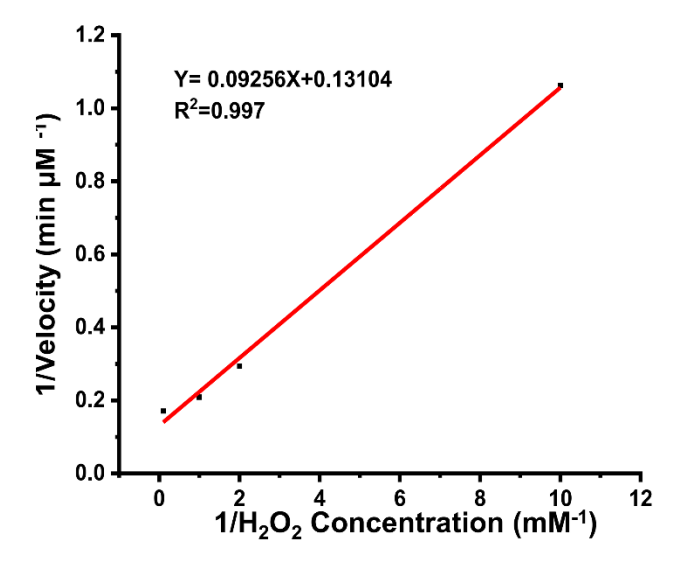


Figure S6. The double reciprocal of Michaelis–Menten fitting curve plotting the initial velocities within the first 15 min against H_2O_2 concentrations, TMB = 1 mM, Fe/Co-MIL-88(NH₂) = 5 μ g/ml in 200 mM NaAc-HAc buffer at pH 7.4.

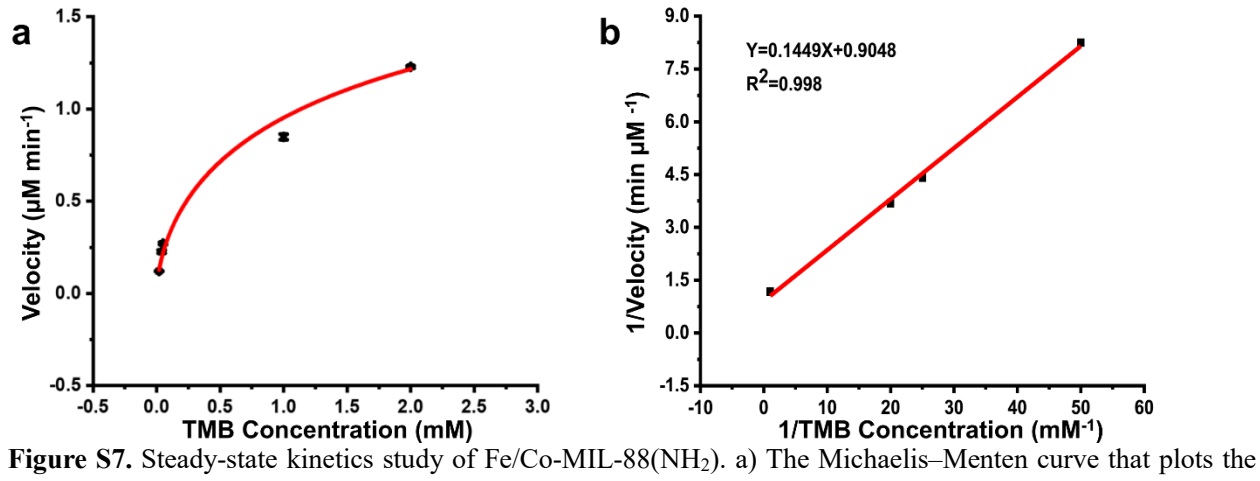


Figure S7. Steady-state kinetics study of Fe/Co-MIL-88(NH₂). a) The Michaelis–Menten curve that plots the initial •OH generation velocities within the first 15 min against TMB concentrations. b) The double reciprocal of Michaelis–Menten fitting curve using data shown in a), $H_2O_2 = 1$ mM, Fe/Co-MIL-88(NH₂) = 5 μ g/ml in 200 mM NaAc-HAc buffer at pH 4.1.

4. Optimization of the cascade enzyme reaction.

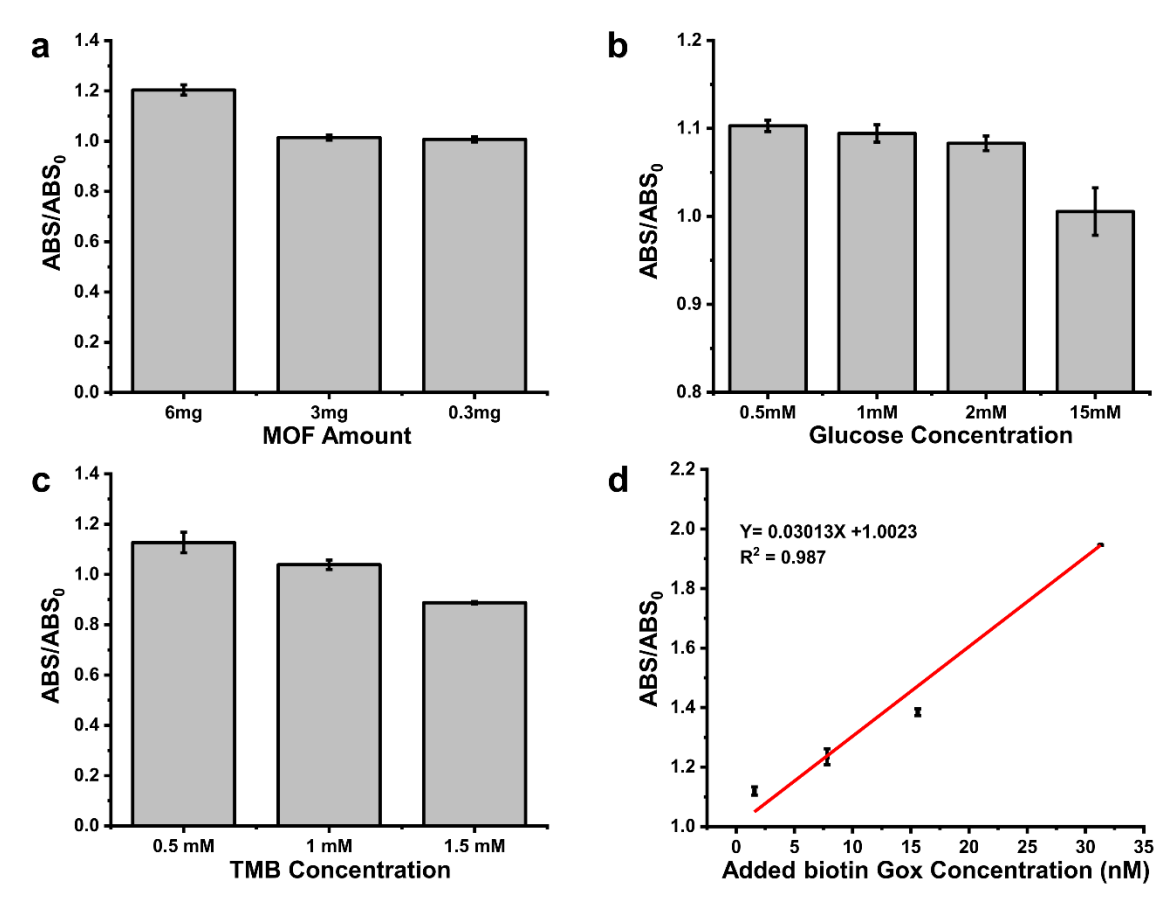


Figure S8. Optimization of the cascade enzymatic reaction in 200 mM NaAc-HAc buffer at pH=4.1. a) Absorbance signal change with the addition of different amount of the MOF while keeping TMB and glucose at 1.0 and 2.0 mM, respectively. b) Absorbance signal change with the addition of different concentrations of glucose, while keeping TMB at 1.0 mM and MOF amount as 3.0 mg per reaction, respectively. c) Absorbance signal change with the addition of different concentrations of TMB, while keeping glucose at 2 mM and MOF amount as 3.0 mg per reaction. d) Detection of biotinylated GOX at the optimized enzyme and substrate conditions: MOF amount = 3.0 mg, TMB = 0.50 mM, Glucose = 0.50 mM. Reaction time = 30min.

5. Aptamer conjugation and detection comparison with ELISA.

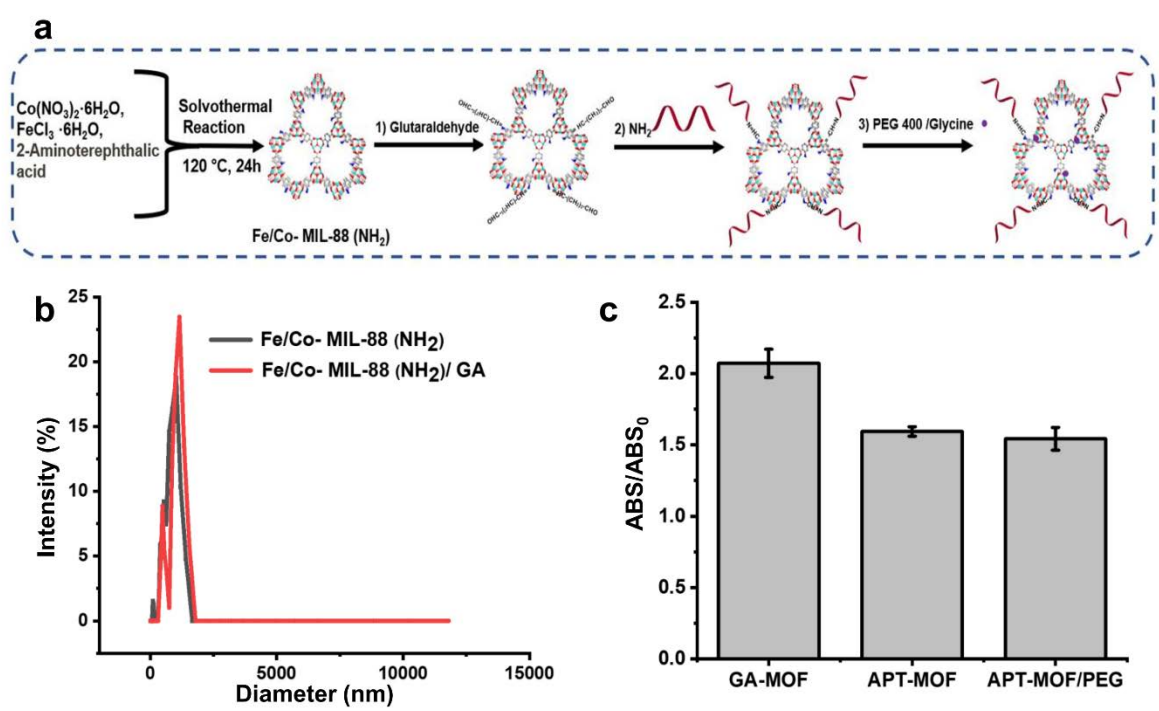


Figure S9. a) Conjugation of Fe/Co-MIL-88(NH₂) with the anti-CD63 aptamer through glutaraldehyde followed by passivation of the surface active groups with PEG 400 and glycine. b) Dynamic Light Scattering measurement of Fe/Co-MIL-88(NH₂) before and after reaction with glutaraldehyde. c) Peroxidase activity assessment after reaction with glutaraldehyde (GA-MOF), aptamer modification (APT-MOF), and surface passivation (APT-MOF/PEG). TMB = 1 mM, MOF = 0.7 mg/ml, $H_2O_2 = 0.5$ mM, in 200 mM NaAc-HAc buffer at pH = 4.1. Reaction time = 15 min. Background: $H_2O_2 = 0$ mM.

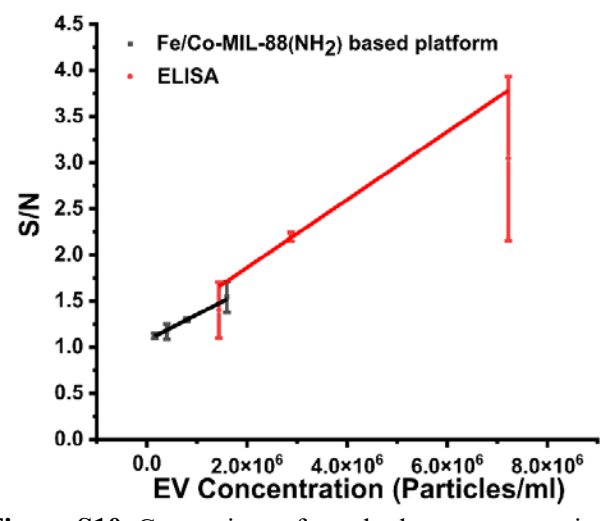


Figure S10. Comparison of standard curves measuring spiked EVs using conventional ELISA vs. the Fe/Co-MIL-88(NH₂) based EV detection platform. The LODs obtained from the ELISA and the Fe/Co-MIL-88(NH₂) based EV detection platform were 4.6×10^6 p/mL an 7.8×10^4 p/mL, respectively. Anti-CD9 and anti-CD81 were applied as capturing antibodies, anti-CD63 was applied as detection antibodies, and the secondary antibody conjugated with HRP was employed for signal development in the conventional ELISA.